

Porous Bilayer Electrode-Guided Gas Diffusion for Enhanced CO₂ Electrochemical Reduction

Yucheng Wang, Hanhui Lei, Hang Xiang, Yongqing Fu, Chenxi Xu, Yin Zhu Jiang, Ben Bin Xu,* Eileen Hao Yu,* Chao Gao,* and Terence Xiaoteng Liu*

Comparing with the massive efforts in developing innovative catalyst materials system and technologies, structural design of cells has attracted less attention on the road toward high-performance electrochemical CO₂ reduction reaction (eCO₂RR). Herein, a hybrid gas diffusion electrode-based reaction cell is proposed using highly porous carbon paper (CP) and graphene aerogels (GAs), which is expected to offer directional diffusion of gas molecules onto the catalyst bed, to sustain a high performance in CO₂ conversion. The above-mentioned hypothesis is supported by the experimental and simulation results, which show that the CP + GA combined configuration increases the Faraday efficiency (FE) from ≈60% to over 94% toward carbon monoxide (CO) and formate production compared with a CP only cell with Cu₂O as the catalyst. It also suppresses the undesirable side reaction—hydrogen evolution over 65 times than the conventional H-type cell (H-cell). By combining with advanced catalysts with high selectivity, a 100% FE of the cell with a high current density can be realized. The described strategy sheds an extra light on future development of eCO₂RR with a structural design of cell-enabled high CO₂ conversion.

decarbonization manifestos in the last few decades, with the advantages of producing high value chemical products and energy feedstock.^[1] Among all technologies envisaged by far, electrochemical reduction of CO₂ has been recognized as a distinguished candidate on the road toward highly efficient conversion of CO₂ at scale-up applications because of its controllable process,^[2] moderate reactions under ambient conditions,^[3,4] and highly designable and productive outputs (e.g., carbon monoxide (CO), CH₄, C₂H₂, C₂H₄, formic acid (HCOOH), methanol (CH₃OH), and ethanol (CH₃CH₂OH)).^[5] However, a number of challenges in the electrochemical CO₂ reduction reaction (eCO₂RR) remain to be tackled, e.g., inertness of CO₂,^[6] which requires a high overpotential (OP) to be kinetically activated, its low solubility in electrolyte^[7] that easily lead to low efficient reaction, desired yield selection process for mixed productions through enhance selectivity^[8] and catalytic activity,^[9] and durability of the reaction/system^[10,11] especially at a scale-up process.

Current researches in eCO₂RR mostly focus on developing novel catalysts with designed morphology,^[12] crystallization,^[13]

1. Introduction

Carbon dioxide (CO₂) capture and utilization have been frequently described as promising technical routes in the numerous

Dr. Y. Wang, H. Lei, Prof. Y. Fu, Prof. B. B. Xu, Dr. T. X. Liu
Faculty of Engineering and Environment
Northumbria University
Newcastle Upon Tyne NE1 8ST, UK
E-mail: ben.xu@northumbria.ac.uk; terence.liu@northumbria.ac.uk

Dr. H. Xiang, Prof. C. Xu, Prof. E. H. Yu
School of Engineering
Newcastle University
Newcastle Upon Tyne NE1 7RU, UK
E-mail: E.Yu@lboro.ac.uk

Prof. C. Xu
Department of Materials Science and Engineering
Hefei University of Technology
Hefei 230009, P. R. China

The ORCID identification number(s) for the author(s) of this article can be found under <https://doi.org/10.1002/aesr.202100083>.

© 2021 The Authors. Advanced Energy and Sustainability Research published by Wiley-VCH GmbH. This is an open access article under the terms of the Creative Commons Attribution License, which permits use, distribution and reproduction in any medium, provided the original work is properly cited.

DOI: 10.1002/aesr.202100083

Prof. Y. Jiang
School of Materials Science and Engineering
State Key Laboratory of Clean Energy Utilization
Zhejiang University
Hangzhou 310027, P. R. China

Prof. E. H. Yu
Department of Chemical Engineering
Loughborough University
Loughborough LE11 3TU, UK

Prof. C. Gao
MOE Key Laboratory of Macromolecular Synthesis and Functionalization
Department of Polymer Science and Engineering
Key Laboratory of Adsorption and Separation Materials and Technologies of Zhejiang Province
Zhejiang University
38 Zheda Road, Hangzhou 310027, P. R. China
E-mail: chaogao@zju.edu.cn

and particle size,^[14] to realize an enhanced selectivity and Faraday efficiency (FE) for a desired eCO₂RR process/product. The eCO₂RR is usually taken place within a conventional H-cell^[15,16] consisting of a working electrode made by porous materials, e.g., carbon paper (CP)^[17] and metal mesh.^[18] Recent advancement in electrode design has achieved gas diffusion electrode (GDE) to enhance the mass transfer in eCO₂RR, where the gas diffusion in porous media leads to the retention of CO₂ within the electrode to extend the saturation on the catalyst bed. Therefore, a desired mass transfer of CO₂ can be facilitated to limit hydrogen evolution and improve reaction rate of eCO₂RR for a higher FE and selectivity. Xiang et al. reported a porous conductive CP-based GDE to achieve more than fivefold in efficiency (current density) of that from the conventional H-cell.^[19,20] Further developments provided perspectives to optimize the mass transfer for high conversion rate of eCO₂RR by designing the surface/interface and geometrical features of electrodes;^[21] for example, De Arquer et al.^[22] developed a catalyst: ionomer bulk heterojunction GDE design to achieve higher CO₂ electrochemical reduction with an ethylene partial current density of 1.3 amperes per square centimeter at 45% cathodic energy efficiency.

Theoretical understanding on the mass transfer in porous media remains to be fully explored, because it could be influenced by many factors, e.g., catalyst, electrode material, electrolyte, electrode assembly, and the molar concentration of the reactant gas along the electrocatalyst surfaces. However, it has been well known that the gas diffusion in porous media can lead to the retention of CO₂ within the electrode to extend saturation on the catalysts, thus enhancing reaction kinetics, FE, and selectivity.

Here, we introduce a porous hybrid bilayer design with interface of two porous materials, aiming to create alternative mass transfer by establishing the circulation/diffusion subcycle for an improved eCO₂RR performance. We first design and compare four types of electrochemical reactors (Figure S1, Supporting Information), with the first design is a compact H-cell (Figure S1a and S5a, Supporting Information). Comparing with the conventional H-cell,^[16] this compact H-cell presents incremental optimization by offering more areas for the working electrode but less spaces between cathode and anode (≈ 1 cm). This can result into a lower electrolyte resistance (causing an OP) for electrochemical behavior.^[23] This type of gas supply will inevitably enable poor CO₂ transfer caused by the low solubility of CO₂ in electrolyte,^[24] whereas hydrogen evolution reaction (HER) will also happen and reduce the CO₂ reduction efficiency.^[25,26] Meanwhile, CO₂ supplying method based on the idea of “bubbling into electrolyte” will be likely to occur to destabilize the system, where some CO₂ bubbles will stick on the surface of working electrode and block the pathway of proton transfer to the catalyst surface (Figure S2, Supporting Information). These will yield less electrode areas for reaction, thus leading to a significantly decrease in current density.

The core structure for the second design (CP-cell) is a conventional CP-based GDE, which serves as a current collector and foundation to support the catalyst layer (Figure 1a). The integrated CP-cell design is shown in Figure 1c and Figure S1b, Supporting Information, where the catalyst layer with an average thickness of 10 μm is homogeneously attached on the CP surface

(Figure 1e). However, the CP will degrade after a long-term reaction, and the permeation of water easily occurs in this type of cell to trigger HER as well as the blockage of CO₂ mass transfer pathway. In addition, an inhomogeneous CO₂ gas flow is often observed in CP-based GDE design due to some of the above-mentioned reasons.

Graphene aerogel (GA) has been considered as a promising electrode material for different scenarios, particularly for its bespoke porosity and stability (Figure S3a, Supporting Information), etc. Our group previously developed a direct methanol fuel cell (DMFC) technology with an enhanced mass power density by replacing CP with GA.^[27] The concept of GA GDE is introduced in the third design (Figure S4a, Supporting Information) with an integrated cell design (GA-cell) shown in Figure S1c and S4b, Supporting Information, where the GA is inserted in the chamber to allow CO₂ to diffuse within the highly porous GA rather than passing through the empty chamber. The high porosity of GA offers a large surface area and a reasonably good conductivity ($\approx 10 \text{ S cm}^{-1}$),^[27] which make it a suitable material as a foundation to host catalyst. Moreover, the 3D structure of GA could resist the permeation of electrolyte effectively. It should be noted that the high roughness on GA's surface could be problematic during the coating process for catalyst, even at a higher loading of 5 mg cm⁻² or after surface treatment, thus leading to a coarse structure and exposing the GA to the electrolyte (Figure S4a and S6c, Supporting Information).

Next, we create a porous hybrid bilayer design (GACP-cell) by practically combining GA (without catalyst, inset of Figure 1e) to the CP GDE. A schematic of this bilayer GDE configuration and an integrated cell design are shown in Figure 1b,d, where GA fills the gas chamber with a very gentle pressure ($\approx 1 \text{ N cm}^{-2}$) applied from the CP to ensure an intimate contact, and the current collector is attached to CP, which is the same construction to the CP-cell for the purpose of maintaining the same overall device resistance to avoid possible interruption to the charge transfer. Electrochemical impedance spectroscopy (EIS) is utilized to assess all GDE cells prior to the CO₂RR testing, and the Nyquist plots (Figure S7, Supporting Information) indicate that all cells display a similar value of R_{ct} , suggesting there is ignorable charge transfer in the following CO₂RR testing for all GDE cells.

An interface effect is expected to increase the mass transfer of CO₂ with a guided diffusion on the catalyst layer (Figure 1f). We next utilized a 3D printing technique to create the parts with the design details of GACP-cell (Figure 1g,i and Figure S1d, Supporting Information) and then fully assembly of the device (Figure 1j). The GACP-cell consists of three chambers. The gas chamber in the left-hand side contains GA, where the CO₂ flows into gas chamber, diffuses through GA and then CP, and finally reaches to the catalyst layer. The middle chamber is filled with catholyte, where the cathode coated with catalyst (Figure 1h) is exposed to the catholyte, and a reference electrode is inserted in this chamber. The right chamber is the anode chamber with anolyte and the inserted counter electrode (Pt wire). A cation exchange membrane is placed between the anode and cathode chambers to allow H⁺ to pass through. All the components with gaskets are firmly connected and sealed to ensure a good contact without any leakage. The whole cell was designed to

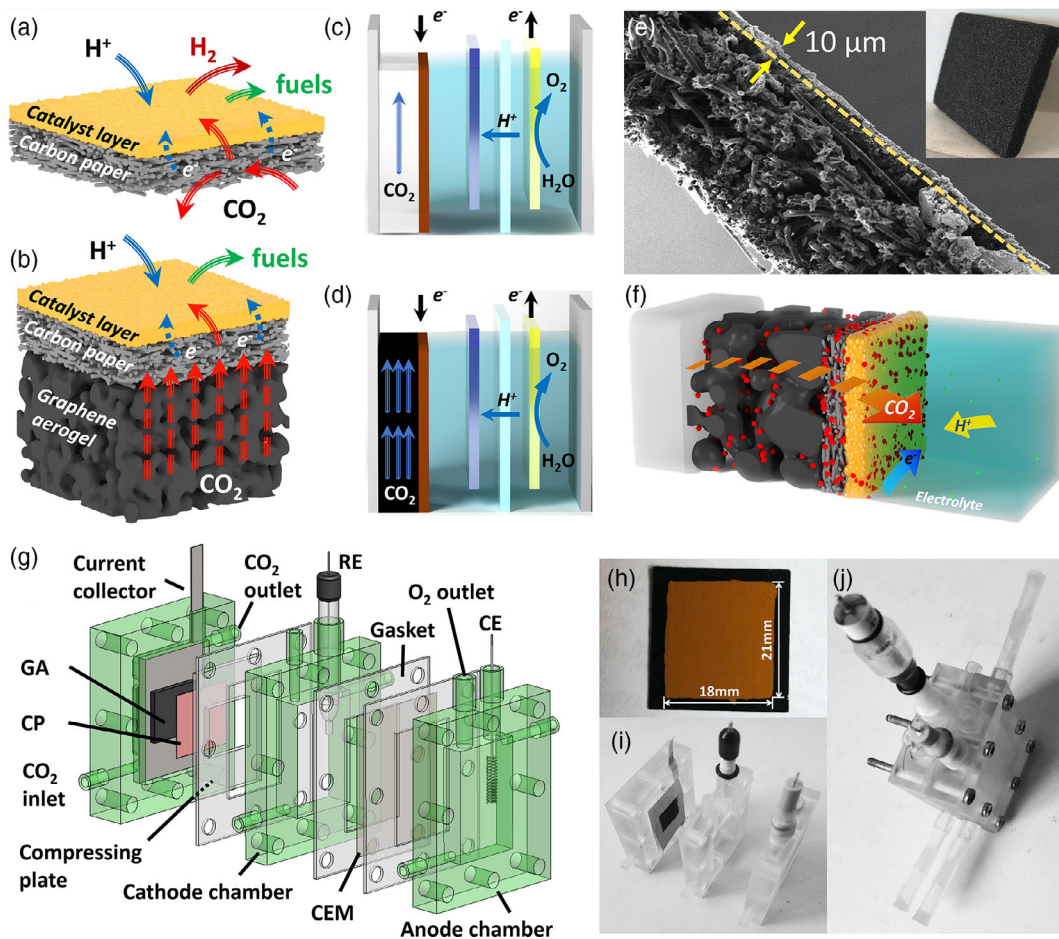


Figure 1. Schematic illustrations of design for a) CP-electrode and b) GACP-electrode. Integrated design for c) CP-cell and d) GACP-cell; components' arrangements from left to right are gas chamber (white: gas channel for CP-cell and black: GA for GACP-cell), catalyst-coated CP (brown), reference electrode (blue) in catholyte, ion exchange membrane (light blue), and counter electrode (yellow) in anolyte. e) Cross-sectional view of bilayer with catalyst layer and GA (insertion). f) CO₂ mass transfer pathway, CO₂ transfer through GA (black), CP (gray), and catalyst layer (yellow). The fabrication of GACP-cell with g) multicomponents, h) top view of bilayer with coated catalyst, i) disassembled, and j) assembled cells.

reduce the electrolyte resistance (more details can be found in Experimental Methods, Supporting Information).

As the pore sizes in the CP and GA are larger than 10 μm, the CO₂ mass transfer in these two media can only be through gas flow. When CO₂ approaches a catalyst layer, a gas concentration gradient is generated near the catalyst layer as a result of gas diffusion, which can be predicted by Fick's second law.^[28]

$$\frac{\partial C}{\partial t} = D_a \frac{\partial^2 C}{\partial x^2} \quad (1)$$

where C refers to the CO₂ molar concentration (mol L⁻³), t is the time (s), D_a is the molecular diffusion coefficient in air (L² s⁻¹), and x is the distance along the axis of flow (L). Compared with the CP-cell, the GA-cell shows a constant CO₂ flow before approaching to the catalyst layer, which will increase CO₂ molar concentration with a homogenous distribution. The interface between the CP and GA layers plays a key role by acting as a boundary for the gas transfer, where the occurrence of sub-circulation is

expected to enhance the CO₂ gas diffusion and prevent the water penetration.

To explore and compare the mass transfer for the cell designs, COMSOL simulation of real time CO₂ molar concentrations along the cathode catalyst layer has been performed for the CP-cell, GA-cell, and GACP-cell (Figure 2a-c). The simulations are set based on the following assumptions: 1) There is no thermal expansion; 2) sufficient CO₂ is supplied from the inlet; 3) CO₂ is reacted immediately once arriving the catalyst layer; and 4) the morphology of membrane is sustained throughout the reaction with no residual stress to cause the rupture. Detailed parameters, settings, and conditions in the simulations are summarized in Table S1 and S2, Supporting Information.

The simulation outcomes show that the CO₂ molar concentration for CP-cell (Figure 2a) is generally lower than those from the other cells. The GA-cell (Figure 2b) appears to have a high CO₂ molar concentration around the inlet with a fast-decreasing gradient, and the rest of the electrode shows a nearly constant CO₂ molar concentration, which is slightly higher than that of CP-cell. The GA increases CO₂ gas diffusion within the electrode and

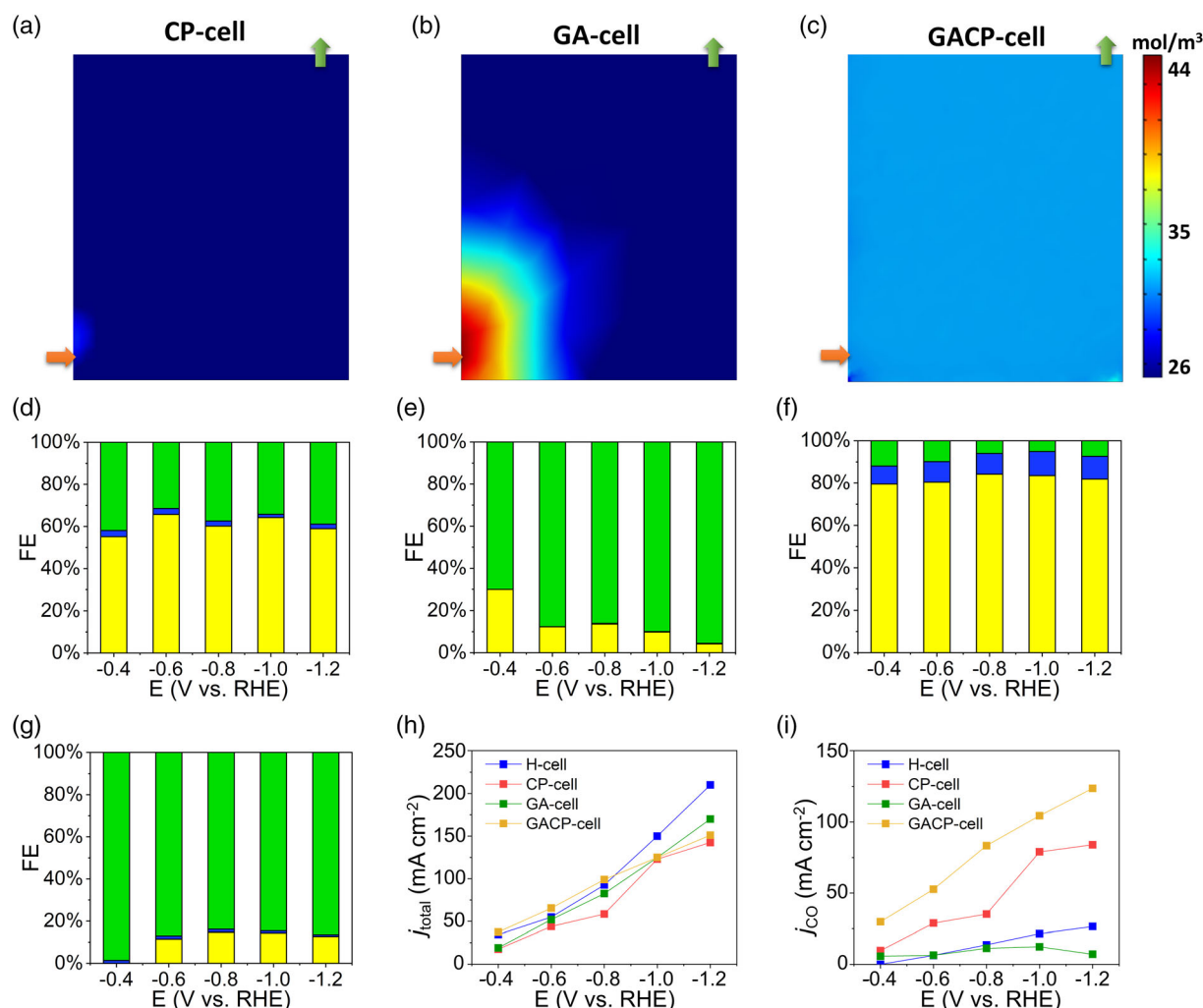


Figure 2. COMSOL simulation on CO₂ molar concentration along the cathode catalyst layer for a) CP-cell, b) GA-cell, and c) GACP-cell. Faradaic efficiency profiles of d) CP-cell, e) GA-cell, f) GACP-cell, and g) H-cell using Cu₂O catalyst in 1 M KOH electrolyte of eCO₂RR with products, including CO (yellow, bottom), formate (blue, middle), and H₂ (green, top). h) Total current density for results in (d-g). i) Current density of CO for results in (d-g).

reduces its transferring speed prior to leave the chamber for a higher reaction efficiency. The CO₂ molar concentration is effectively enhanced in the GACP-cell, because the CO₂ feedstock supplies reactant more evenly through its body to the catalyst layer. An explicit improvement in the uniformity of CO₂ molar concentrations is obtained (Figure 2c) along the electrode surface, in which a homogeneous distribution is observed. A higher FE value and a better eCO₂RR performance can be realized due to the improved mass transfer from the abundant supply of reactant.

The catalyst system used in this research is homemade Cu₂O and commercially available antimony tin oxide (ATO) nanoparticles. It has been reported that the Cu₂O has a high electrocatalytic activity to produce CO with a high value of FE under ambient conditions,^[10,29] and antimony oxide and tin oxide are reported to have good activity on generating formate.^[30] Therefore, ATO is used to assess high value of FE of formate for both gas and liquid productions. These catalysts were coated onto the surface of CP with a loading of 5 mg cm⁻².

The FE results of CP-cell, GA-cell, GACP-cell, and H-cell are shown in Figure 2d-g (more information in Table S3–S6, Supporting Information), where the green bars represent H₂ generated from HER, the yellow bars represent CO, and the blue bars represent formate. The total current density and current density of CO generated from Autolab potentiostat are shown in Figure 2h,i (more information in Table S7 and S8, Supporting Information). It is shown in Figure 2g that the HER dominates the reaction in the H-cell, with a small amount of CO and formate produced at –0.4 V versus reference hydrogen electrode (RHE). At low potentials, the main product is hydrogen, as the OP of HER in the alkaline environment is near to 0 V versus RHE. There is an increase in the FE value for the CO when increasing potential, but that of the formate remains unchanged. For the H-cell, in the aqueous media, CO₂ gas is dissolved in catholyte and form CO₂(aq.), which is then transferred from the catholyte to surface of the catalyst layer.^[20] A low solubility will limit CO₂ supply, and thus, the HER will happen when there is the absence of CO₂, eventually lead to a low FE of carbonaceous products.^[25]

Increasing the solubility of CO₂ in electrolyte has been seen as one of the promising means to enhance CO₂ mass transfer in H-cell, in which CO₂ was supplied under high pressure and high temperature to address the solubility issues.^[20] However, the nonambient processing conditions may destabilize the system and are less feasible for scale-up application. A re-configuration of the CO₂ liquid supplying is desirable for mass transfer problem from the above-mentioned perspectives. Although the above-mentioned solutions may improve the mass transfer by enhancing the solubility of CO₂, it is theoretically relied upon CO₂ in liquid phase devices for eCO₂RR. In addition, K⁺ in electrolyte would be easily bound onto the electrode and prohibit CO₂ diffusion,^[20,31] which leads to the overall reaction turning into water splitting.

The CP-cell shows a much higher FE value of CO than that of H-cell, as shown in Figure 2d. Its FE values of CO at the potentials of -0.4, -0.6, -0.8, -1.0, and -1.2 V are 55.13%, 65.71%, 60.19%, 64.23%, and 58.93%, respectively, and the FEs of formate at the potentials of -0.4–0.6 V, -0.8, -1.0, and -1.2 V are 2.95%, 2.83%, 2.42%, 1.54%, and 2.19%, respectively. The decreased FE values toward HER are resulted from the minimized exposure of CP and the creation of three phase boundaries, which improve the CO₂ mass transfer. As shown in Figure 1e of the cross-sectional view of the CP GDE, the catalyst formed a uniform layer with a thickness of 10 μm, and the CP was pre-treated with a polytetrafluoroethylene (PTFE) layer to block the water. In this configuration, the CO₂ gas can directly reach the catalyst layer, thus overcoming the gas diffusion limitations in the electrolyte.

Among these three new devices, the GA-cell presents the lowest FE value of formate, as shown in Figure 2e. A large amount of graphene is exposed while printed with the catalyst ink, and this yields an inhomogeneous catalyst layer. Even with a high catalyst loading of 5 mg cm⁻² (Figure S6c, Supporting Information), there is still exposure of GA “skeleton” (graphene), which takes part in HER. Moreover, the organic-friendly GA may absorb the formate and reduce its concentration, which can be detected in the ion chromatography (IC) test. The FE values of CO are 29.97%, 12.34%, 13.62%, 9.86%, and 4.17% at the potentials from -0.4 to -1.2 V.

Once a plain GA was attached at the back of the CP GDE, the GACP-cell is constructed. In Figure 2f, the FE values of CO are enhanced to 79.58%, 80.41%, 84.20%, 83.54%, and 81.91%, and the FE values of formate are increased to 8.47%, 9.73%, 9.81%, 11.35%, and 10.73%, respectively, at -0.4 to -1.2 V potentials for the GACP-cell. This new cell suppressed the FE values of H₂ from HER to 11.95%, 9.86%, 5.99%, 5.11%, and 7.36%, at -0.4 to -1.2 V, which is a dramatic 11-times improvement than those of the H-cell. Compared with the CP-cell, the GACP-cell presents higher current density (Figure 2h) in the potential ranged from -0.4 to -0.8 V versus RHE, and the H-cell shows a higher current density at a larger negative potential. This shows the evidence that the HER is dominated the reaction. From the current density of the desired product CO (Figure 2i), it is obvious that the GACP-cell presents the highest current density for CO production. The above-mentioned experimental results confirm our prospective that the improvement in mass transfer induces a higher CO₂ molar concentration, and it also agrees well with the simulation results.

COMSOL simulation results of OP distribution along the cathode catalyst layers for CP-cell, GA-cell, and GACP-cell are presented in Figure S8, Supporting Information. All results show a mixed distribution of the OP ranges from -0.2 to 0 V. The HER occurs at OP near to 0 V. Generation of CO and formate from eCO₂RR provides the OPs of -0.11 and -0.20 V versus RHE (pH = 7),^[32] respectively. An increasing trend of absolute value of OPs can be observed with the sequence order for the CP-cell, GA-cell, and then GACP-cell. This means higher productions of CO and formate for both GA-cell and GACP-cell, which agrees well with our experimental results. However, the GA-cell shows a different profile for both results of CO₂ molar concentration and OP simulations, due to the unavailability of defining the exposure of graphene on GA in COMSOL simulations.

To verify the stability for CP-cell and GACP-cell, we performed the eCO₂RR under -1.0 V versus RHE in 1 M potassium hydroxide (KOH) with a constant CO₂ gas supply (15 mL min⁻¹). The durability test results for these cells are shown in Figure 3. The long-term experiment had been conducted for 4 h first and then paused to analysis the catholyte for liquid products. Then, a new solution of 1 M KOH was added inside, and the reaction was continued for another 4 h. The tail gas was collected using a gas bag to analyze the gaseous products during each 4 h electrochemical test. From the reaction efficiency chronoamperometry (CA) diagram in Figure 3a and the FE results shown in Figure 3b, the FE values of CO are reduced from 63.28% to 22.93%, and the FE values of H₂ are increased from 34.92% to 75.53% at -1.0 V for the CP-cell. The FE values of CO are reduced from 83.36% to 79.27%, and the FE value of H₂ increased from 5.74% to 12.50% at -1.0 V for the GACP-cell. It is found that the GACP-cell presents a better stability than the CP-cell, due to the homogenous distribution of CO₂ induced by porous bilayer. Meanwhile, the catalyst layer is protected from peeling off from the CP during the reaction, which leads to less carbon exposed to the electrolyte. GA also prevents the permeation of electrolyte through the gas diffusion layer (GDL), which leads the CP lost its GDE function.

The system's durability could also be influenced by the competing reaction of HER. After durability test, it is found that the catholyte partially permeated through the CP GDE, which leads to a higher FE value for the CP-cell toward HER. GA's hydrophobic surface delays the liquid penetration, which sustains a high FE value toward eCO₂RR. The catalyst morphology of GACP-cell before durability tests is characterized and shown in Figure 3c and Figure S6a, Supporting Information, with the X-ray diffraction (XRD) results of Cu₂O-coated CP in Figure S6b, Supporting Information. The scanning electron microscopy (SEM) image of electrode surface after durability test is shown in Figure 3d. Cu₂O nanocubes were found to uniformly distribute on the CP before and after the durability test, which indicates that the structure of catalyst layer has not been destroyed without much loss of the catalyst loading. However, Cu₂O appears to be slightly corroded because of electrochemical corrosion, which could reduce its catalyst properties. This phenomenon-could explain the decrease in the FE value in the GACP-cell. The same catalyst corrosion is also observed on H-cell and CP-cell electrodes after durability test (Figure S9, Supporting Information), and this indicates that the catalysts degradation did not influence the GDL discovery.

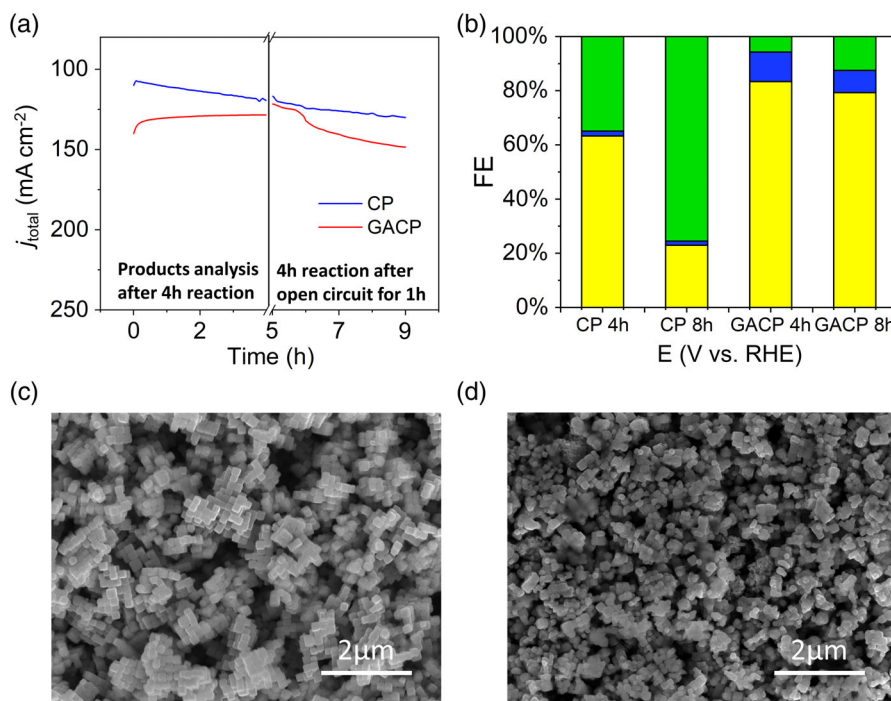


Figure 3. Durability test results under 1 V versus RHE of CP-cell and GACP-cell. a) CA plot and b) FE graph for CP- and CPGA-cell at fourth and eighth hours for durability test. c,d) SEM of the catalyst surface of GACP-cell before and after durability test.

Detailed data of durability test and relevant random error are listed in Table S9, Supporting Information.

We then use the commercially available ATO nanoparticles as the eCO₂RR catalyst to investigate the feasibility of using GACP-

cell to produce formate, which is in a liquid form. The performance of four types of cells is presented in Figure 4. Within the potential range of -0.4 to -1.2 V versus RHE, the H-cell (Figure 4a) presents the lowest FE values of formate and CO

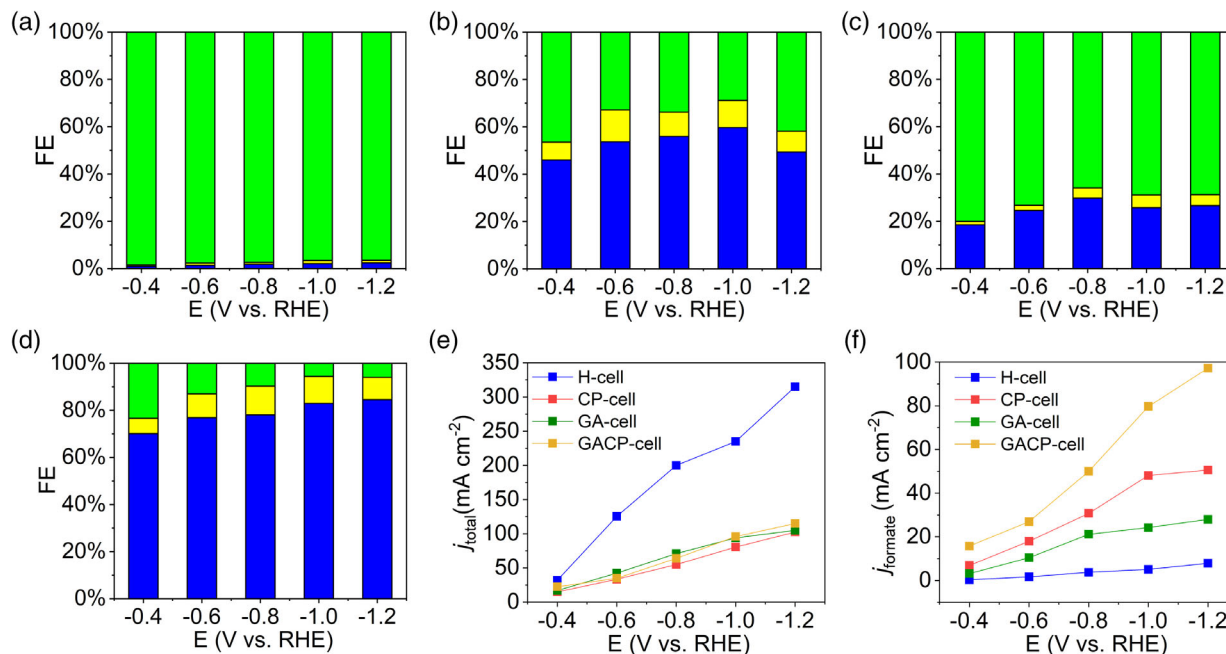


Figure 4. Faradaic efficiency profiles of a) H-cell, b) CP-cell, c) GA-cell, and d) GACP-cell using ATO catalyst in 1 M KOH electrolyte of eCO₂RR with products, including formate (blue, bottom), H₂ (green, top), and CO (yellow, middle). e) Total Current density for results in (a-d). f) Current density of formate for results in (a-d).

but the highest current density, because the HER dominates the reaction. The CP-cell (Figure 4b) shows the higher FE values toward eCO₂RR, and the GACP-cell obtained the highest FE values from all potentials. From the result, the FE values of formate in the CP-cell are 45.98%, 53.66%, 55.91%, 59.71%, and 49.36% at a potential range from -0.4 to -1.2 V, where the FE values of formate in the GACP-cell (Figure 4d) are 70.10%, 76.91%, 78.11%, 82.98%, and 84.54%, respectively. The full set of data for FEs and random errors is listed in Table S10–S15, Supporting Information. For the GA-cell (Figure 4c), the exposed skeleton will only benefit water splitting, and a lower FE value of eCO₂RR was obtained.

Figure 4e, f shows the total current density and formate partial current density. The H-cell presents the highest current density toward HER and the lowest current density of formate product. The other devices present similar current densities, and the GACP-cell shows the highest current density of formate. The results agree with our simulation results and confirm the results from using Cu₂O catalyst.

In conclusion, we demonstrate to achieve a high FE of over 94% for CO and formate generation by improving the mass transfer of CO₂ reactant within the electrode. Results from the GACP-cell configuration show the highest CO₂ molar concentration along the electrode surface. Using two types of catalysts, it has been confirmed that our GACP-cell can be applied for both gas and liquid systems. The influence of CO₂ supply is mainly due to device design, which can enhance overall eCO₂RR performance and realize low cost and high efficiency eCO₂RR. This study also shed a light on improving eCO₂RR from engineering design point of view. By combining with advanced catalysts, a low energy consumption robust, industrialization possible CO₂ to fuel conversion system could become a reality.

2. Experimental Section

Device Fabrication and Assembly: SOLIDWORKS software was used for all electrochemical cell parts design. The drawings of all four type cells are presented in Figure S5, Supporting Information, and Figure 1g. Formlabs Form 2 3D printer with photopolymer resin (FLGPCL04) was used to print gas chamber, catholyte chamber, and anode chamber. The inner size of two electrolyte chambers was 36 × 23 × 10 mm, and the injected electrolyte volume in each chamber was 7 mL. A small gap was designed above the chamber to avoid electrolyte spillage. For working electrode current supplying issue, conductive resin was used to connect CP and titanium wire in H-cell. For CP-cell, GA-cell, and GACP-cell, hollowed current collector plate and working electrode were compressed by hollowed compressing plate (area for middle gap: 2 cm²).

Two materials were applied as the GDL. CP (product code H23C6) was purchased from Freudenberg Ltd. GA was prepared based on the procedures reported in our previous published work.^[27] The CP and GA were cut into 18 × 21 mm² as the working electrode. For GACP-cell, the GA and CP were compressed and assembled in device. Detailed preparation process for the GDE followed the same route for all the cells, and the catalysts were coated on CP using hand brush and using spray gun for GA. The catalysts on GDEs as well as the cross section of the electrodes were characterized using XRD and SEM combined with energy-dispersive spectroscopy (SEM/EDX).

Electrochemical Evaluation Methods: All electrochemical results were recorded using potentiostat/galvanostat (Metrohm Autolab PGSTAT204). Reference electrode is converted to RHE using the following equation.

$$E_{\text{RHE}} = E_{\text{Ag/AgCl}} + 0.197 \text{ V} + 0.0591 \text{ V} \times \text{pH} \quad (2)$$

To evaluate the catalysis electrochemical performance for CO₂ reduction reaction, we performed electrochemical tests using different cells, and 1 M KOH and 5 M KOH were used as catholyte and anolyte, respectively. The H-cell was purged with CO₂ (BOC 99.99%) for 30 min before the electrochemical tests, and the pH of catholyte was measured as 13.8 after bubbling. For all the other GDE cells, pre-purge CO₂ into electrolyte is not necessary. The CO₂ gas flow rate during testing was controlled using a flow meter (Cole-Parmer TMR1-010462) with a value of 15 mL min⁻¹.

To analyze eCO₂RR behavior in different cells, we performed the CA tests (Metrohm Autolab PGSTAT128N potentiostat/galvanostat) at -0.4, -0.6, -0.8, -1.0, and -1.2 V versus RHE for 1000 s. The current density (*j*) was recorded, and then, the gas/liquid products were collected for composition analysis using gas chromatography (GC; Shimadzu Tracera GC-2010) with a barrier discharge ionization (BID) detector and IC (equipped with “Metrohm 6.1005.200” column formic acid identification). The FE value of each product was calculated according to Faraday's law.^[4]

$$\text{FE} = \frac{\alpha n F}{Q} \quad (3)$$

where α is the number of electrons transferred for reactants (e.g., $\alpha = 2$ for reduction of CO₂ to HCOO⁻), n is the moles of the desired product, F is Faraday's constant (96 500 Cmol⁻¹), and Q means the total passed charge.

Two sets of the cells were manufactured, and all above-mentioned experiments were performed three times with random error, which is shown in brackets in Table S3–S7 and S9–S14, Supporting Information, which indicates sample standard deviation. The current density (*j*) values in Table S8 and S15, Supporting Information, are calculated using the following equation.

$$j_a = j_{\text{total}} \times \text{FE}_a \quad (4)$$

where j_a is the current density of a specific product, and FE_a is the Faradaic efficiency of this product. No experimental error is included in Table S8 and S15, Supporting Information, because it is the calculated value.

Supporting Information

Supporting Information is available from the Wiley Online Library or from the author.

Acknowledgements

This work was supported by the UK Engineering Physics and Science Research Council (Grant Nos. EP/S032886/1, EP/P026435/1, and EP/N007921).

Conflict of Interest

The authors declare no conflict of interest.

Data Availability Statement

The data that supports the findings of this study are available in the supplementary material of this article.

Keywords

CO₂ reduction reaction, gas diffusion electrodes, graphene aerogels, mass transfer

Received: April 8, 2021
Revised: April 9, 2021
Published online: June 7, 2021

- [1] a) M. Bui, C. S. Adjiman, A. Bardow, E. J. Anthony, A. Boston, S. Brown, P. S. Fennell, S. Fuss, A. Galindo, L. A. Hackett, J. P. Hallett, H. J. Herzog, G. Jackson, J. Kemper, S. Krevor, G. C. Maitland, M. Matuszewski, I. S. Metcalfe, C. Petit, G. Puxty, J. Reimer, D. M. Reiner, E. S. Rubin, S. A. Scott, N. Shah, B. Smit, J. P. M. Trusler, P. Webley, J. Wilcox, N. Mac Dowell, *Energy Environ. Sci.* **2018**, *11*, 1062; b) F. M. Baena-Moreno, M. Rodríguez-Galán, F. Vega, B. Alonso-Fariñas, L. F. Vilches Arenas, B. Navarrete, *Energy Sources, A* **2018**, *41*, 1403.
- [2] a) S. Liang, N. Altaf, L. Huang, Y. Gao, Q. Wang, *J. CO₂ Utiliz.* **2020**, *35*, 90; b) Y. Wu, S. Cao, J. Hou, Z. Li, B. Zhang, P. Zhai, Y. Zhang, L. Sun, *Adv. Energy Mater.* **2020**, *10*, 2000588.
- [3] J. Qiao, Y. Liu, F. Hong, J. Zhang, *Chem. Soc. Rev.* **2014**, *43*, 631.
- [4] D. D. Zhu, J. L. Liu, S. Z. Qiao, *Adv. Mater.* **2016**, *28*, 3423.
- [5] a) D. Raciti, C. Wang, *ACS Energy Lett.* **2018**, *3*, 1545; b) T. B. C.-T. Dinh, Md G. Kibria, A. Seifitokaldani, C. M. Gabardo, F. P. G. de Arquer, A. Kiani, J. P. Edwards, P. De Luna, O. S. Bushuyev, C. Zou, R. Quintero-Bermudez, Y. Pang, D. Sinton, E. H. Sargent, *Science* **2018**, *360*, 783; c) T.-T. Zhuang, Y. Pang, Z.-Q. Liang, Z. Wang, Y. Li, C.-S. Tan, J. Li, C. T. Dinh, P. De Luna, P.-L. Hsieh, T. Burdyny, H.-H. Li, M. Liu, Y. Wang, F. Li, A. Proppe, A. Johnston, D.-H. Nam, Z.-Y. Wu, Y.-R. Zheng, A. H. Ip, H. Tan, L.-J. Chen, *Nat. Catal.* **2018**, *1*, 946; d) S. Sen, D. Liu, G. T. R. Palmore, *ACS Catal.* **2014**, *4*, 3091; e) Y. Liu, S. Chen, X. Quan, H. Yu, *J. Am. Chem. Soc.* **2015**, *137*, 11631; f) G. Lu, H. Wang, Z. Bian, X. Liu, *Sci. World J.* **2013**, *2013*, 424617; g) A. J. Garza, A. T. Bell, M. Head-Gordon, *ACS Catal.* **2018**, *8*, 1490.
- [6] a) C.-H. Huang, C.-S. Tan, *Aerosol Air Quality Res.* **2013**, *14*, 480; b) X. Xiaoding, J. Mouljin, *Energy Fuels* **1996**, *10*, 305; c) C. M. Gabardo, C. P. O'Brien, J. P. Edwards, C. McCallum, Y. Xu, C.-T. Dinh, J. Li, E. H. Sargent, D. Sinton, *Joule* **2019**, *3*, 2777.
- [7] a) J. Durst, A. Rudnev, A. Dutta, Y. Fu, J. Herranz, V. Kaliginedi, A. Kuzume, A. A. Permyakova, Y. Paratcha, P. Broekmann, *CHIMIA Int. J. Chem.* **2015**, *69*, 769; b) T. Zheng, K. Jiang, N. Ta, Y. Hu, J. Zeng, J. Liu, H. Wang, *Joule* **2019**, *3*, 265.
- [8] a) S. Nitopi, E. Bertheussen, S. B. Scott, X. Liu, A. K. Engstfeld, S. Horch, B. Seger, I. E. Stephens, K. Chan, C. Hahn, *Chem. Rev.* **2019**, *119*, 7610; b) T. Hatsukade, K. P. Kuhl, E. R. Cave, D. N. Abram, T. F. Jaramillo, *Phys. Chem. Chem. Phys.* **2014**, *16*, 13814.
- [9] a) D. C. Grills, Y. Matsubara, Y. Kuwahara, S. R. Golisz, D. A. Kurtz, B. A. Mello, *J. Phys. Chem. Lett.* **2014**, *5*, 2033; b) H. A. Hansen, J. B. Varley, A. A. Peterson, J. K. Nørskov, *J. Phys. Chem. Lett.* **2013**, *4*, 388.
- [10] W. Zhang, Y. Hu, L. Ma, G. Zhu, Y. Wang, X. Xue, R. Chen, S. Yang, Z. Jin, *Adv. Sci.* **2018**, *5*, 1700275.
- [11] R. Francke, B. Schille, M. Roemelt, *Chem. Rev.* **2018**, *118*, 4631.
- [12] Y. Peng, T. Wu, L. Sun, J. M. V. Nsanzimana, A. C. Fisher, X. Wang, *ACS Appl. Mater. Interfaces* **2017**, *9*, 32782.
- [13] N. Nilius, H. Fedderwitz, B. Gross, C. Noguera, J. Goniakowski, *Phys. Chem. Chem. Phys.* **2016**, *18*, 6729.
- [14] Y. Fu, Y. Li, X. Zhang, Y. Liu, J. Qiao, J. Zhang, D. P. Wilkinson, *Appl. Energy* **2016**, *175*, 536.
- [15] a) X. Chang, T. Wang, Z. J. Zhao, P. Yang, J. Greeley, R. Mu, G. Zhang, Z. Gong, Z. Luo, J. Chen, Y. Cui, G. A. Ozin, J. Gong, *Angew. Chem. Int. Ed. Engl.* **2018**, *57*, 15415; b) A. Engelbrecht, C. Uhlig, O. Stark, M. Hämmerle, G. Schmid, E. Magori, K. Wiesner-Fleischer, M. Fleischer, R. Moos, *J. Electrochem. Soc.* **2018**, *165*, J3059.
- [16] S. Kaneco, K. Iiba, H. Katsumata, T. Suzuki, K. Ohta, *Electrochim. Acta* **2006**, *51*, 4880.
- [17] S. Park, J.-W. Lee, B. N. Popov, *Int. J. Hydrogen Energy* **2012**, *37*, 5850.
- [18] K. Ogura, H. Yano, T. Tanaka, *Catal. Today* **2004**, *98*, 515.
- [19] H. Yang, Q. Lin, C. Zhang, X. Yu, Z. Cheng, G. Li, Q. Hu, X. Ren, Q. Zhang, J. Liu, C. He, *Nat. Commun.* **2020**, *11*, 593.
- [20] H. Xiang, S. Rasul, K. Scott, J. Portoles, P. Cumpson, E. H. Yu, *J. CO₂ Utiliz.* **2019**, *30*, 214.
- [21] N. Wang, R. K. Miao, G. Lee, A. Vomiero, D. Sinton, A. H. Ip, H. Liang, E. H. Sargent, *SmartMat* **2**.
- [22] F. P. G. De Arquer, C.-T. Dinh, A. Ozden, J. Wicks, C. McCallum, A. R. Kirmani, D.-H. Nam, C. Gabardo, A. Seifitokaldani, X. Wang, *Science* **2020**, *367*, 661.
- [23] D. Kopljar, A. Inan, P. Vindayer, N. Wagner, E. Klemm, *J. Appl. Electrochem.* **2014**, *44*, 1107.
- [24] J. Song, H. Song, B. Kim, J. Oh, *Catalysts* **2019**, *9*, 224.
- [25] T. Burdyny, W. A. Smith, *Energy Environ. Sci.* **2019**, *12*, 1442.
- [26] a) K. Junge Puring, D. Siegmund, J. Timm, F. Möllenbruck, S. Schemme, R. Marschall, U. P. Apfel, *Adv. Sustain. Syst.* **2021**, *5*, 2000088; b) S. Garg, M. Li, T. E. Rufford, L. Ge, V. Rudolph, R. Knibbe, M. Konarova, G. G. Wang, *ChemSusChem* **2020**, *13*, 304.
- [27] X. Liu, J. Xi, B. B. Xu, B. Fang, Y. Wang, M. Bayati, K. Scott, C. Gao, *Small Methods* **2018**, *2*, 1800138.
- [28] C. K. Ho, S. W. Webb, in *Gas Transport In Porous Media*, Vol. 20, Springer, New York **2006**.
- [29] a) J. H. Montoya, C. Shi, K. Chan, J. K. Nørskov, *J. Phys. Chem. Lett.* **2015**, *6*, 2032; b) S. Popović, M. Smiljanić, P. Jovanović, J. Vavra, R. Buonsanti, N. Hodnik, *Angew. Chem. Int. Ed.* **2020**, *59*, 14736.
- [30] a) Y. Chen, M. W. Kanan, *J. Am. Chem. Soc.* **2012**, *134*, 1986; b) N. Han, P. Ding, L. He, Y. Li, Y. Li, *Adv. Energy Mater.* **2020**, *10*, 1902338; c) Y. Zhou, R. Zhou, X. Zhu, N. Han, B. Song, T. Liu, G. Hu, Y. Li, J. Lu, Y. Li, *Adv. Mater.* **2020**, *32*, 2000992; d) F. Li, M. Xue, J. Li, X. Ma, L. Chen, X. Zhang, D. R. MacFarlane, J. Zhang, *Angew. Chem.* **2017**, *129*, 14910.
- [31] J. Resasco, L. D. Chen, E. Clark, C. Tsai, C. Hahn, T. F. Jaramillo, K. Chan, A. T. Bell, *J. Am. Chem. Soc.* **2017**, *139*, 11277.
- [32] J. Wu, Y. Huang, W. Ye, Y. Li, *Adv. Sci.* **2017**, *4*, 1700194.